RETRIEVAL OF POLSAR DECOMPOSITION PARAMETERS BASED INFORMATION FOR LAND USE LAND COVER CLASSIFICATION

Nguyen Ba Duy [1], R.S Chatterjee[2]

[1] *Photogrammetry and Remote Sensing Dept,*
Hanoi university of Mining and Geology, Vietnam
Email: basduy@gmail.com
[2] *Geoscience Division, Indian Institute of Remote Sensing, Dehradun, India*
Email: R.S.Chatterjee@.rs.iirs

KEY WORDS: Land use land cover classification, PolSAR, Decomposition, InSAR

ABSTRACT: Land use/land cover (LULC) mapping is of great significance in scientific, scholarly research, planning and management. It is observed that multispectral classification of optical remote sensing data is unable to separate many of the land use land cover classes due to spectral overlapping of these classes. SAR backscattering provides information on dielectric property of the materials, surface roughness and surface geometry of the terrain in general and nature of scattering in relation to polarization of the EM wave (e.g., surface scattering, volume scattering, multiple scattering, odd bounce or even bounce scattering, polarization randomness and anisotropy) in particular which can be utilized to characterize the land use land cover classes. Similarly, repeat-pass inteferometric SAR (InSAR) coherence represents temporal decorrelation property of the scatterers in each pixel which can be utilized to characterize the LULC classes. In the present study, ALOS PolSAR (Full polarization-Quad Pol. Mode) and InSAR (HH polarization – Fine Beam Single) data were used to characterize the LULC classes of part of Dehradun district of Uttarakhand state. Polarimetric decomposition has been performed by different techniques namely Freeman (Surface – Volume – Double bounce scattering), Krogager (Surface – Double bounce – Helical scattering), Cloude-Pottier (Entropy – Anisotropy – Mean scattering angle or H-A-α) for understanding polarization-specific scattering behavior of the LULC classes. InSAR coherence image of a 46-day data pair was generated to characterize the LULC classes with respect to temporal decorrelation property of the scatterers. Subsequently, classification of LULC classes was performed by support vector machine (SVM) algorithm based on the selected polarimetric parameter. Finally, a set of parameters, obtained from different polarimetric decomposition techniques to characterize, scattering behavior of the LULC classes, which is best suited was selected.

INTRODUCTION

In the present day world, Land Use and Land Cover mapping is of great significance in scientific, scholarly research, planning and management. Regional land use pattern reflects the character of interaction between man and environment and the influence of distance and resources based on mankind's basic economic activities.

The classification of PolSAR images has become an important research topic since PolSAR images through ENVISAT ASAR, ALOS PALSAR and RADARSAT-2 were available. Many classification methods for PolSAR and InSAR data have been explored by researchers [1], [2]. Recently some polarimetric decomposition theorems have been introduced [4], [9], and classification methods based on the decomposition results were also explored by some researchers [5], [14], [15]. The polarimetric parameters extracted using the polarimetric decomposition methods are related to the physical properties of natural media and can be used as descriptive features for classifying observed objects. Fusion of physical and textural information derived from various SAR polarizations is helpful to the improvement of classification results [3], [6]. The information from interferometric SAR data indicates the structure and complexity of the observed object. Combined these different capabilities, substantial improvements in LULC classification can be achieved [15], [16]. However, so far most of the classification methods for PolSAR and InSAR data are pixel-based. The performance of pixel-based classification methods is affected by speckles, and it is hard to utilize the abundant information contained in PolSAR and InSAR data by using these methods. Moreover, the results of the pixel-based methods are almost incontinuous raster format maps, which are hardly used to extract objects of interest and update geographical information system database expediently.

The objective of this study is to explore a new method for classification of PolSAR and InSAR data, and to investigate the potential of PolSAR and InSAR data for LULC classification. A novel classification method, polarimetric

decomposition parameters selected, Interferometric SAR, and SVM algorithm, was proposed for the classification of ALOS PALSAR PolSAR and InSAR data. In this method, 9 PolSAR parameters and 1 interferometric coherence image were first extracted by using different polarimetric decomposition methods (Freeman, Krogager and H/A/α) and combined with the elements of the scattering, coherency and covariance matrix to form a multichannel image. Next, during the characterizing image analysis was performed by using training data (sample data) on the different decomposition image of ALOS PALSAR PolSAR data. Meanwhile, a total of 9 classes features were extracted for different decomposition. Then, for classification support vector machine algorithm was used for different decomposition and for PolSAR parameters selection. Finally, the LULC classification result of ALOS PALSAR PolSAR data of different decomposition and combination of the selected PolSAR parameters was compared.

STUDY AREA AND DATA

Study area

The study area chosen for the research is a part of Dehradun district, Uttrakhand, India. The geographic extent of the study area is (30^0 25' 48'' N, 77^0 48' 04'' E) to (30^0 06' 05'' N, 78^0 12'' 37'' E). It has been observed that, Land Cover in this study area was mostly forest which includes close forest, open forest and scrubs. In this area dry river bed, agricultural land and some other land which covered with mango orchard, tea garden was identified. Different crops like mustard, sugar cane, wheat and also other crops in small entities were observed in this study area.

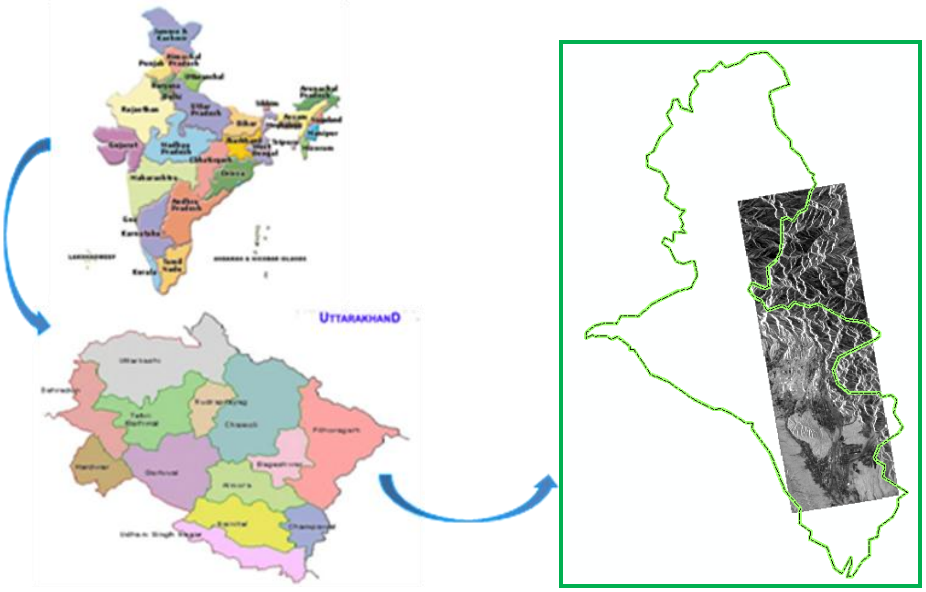

Figure 2.1.1: Study area

Data used

Data used in this study was given in below table:

Table 2.2.1: Data used

N^0	SceneID	Ground Reselution /DPI	Format	Date
ALOS PALSAR (POLSAR)				
1	ALPSRP230860600 (OffNadirAngle="23.1°")	26.4 m	COES	25/05/2010
LANDSAT 7 ETM +				
2	LE71460392009146ASN00	30 m	GeoTIFF	26/05/2009
IRS-P6 LISS-III				

3		23.5 m	TIFF	15/03/2009
TOPOSHEET				
4	53-J/3; 53-F/15 53-J/4; 53-F/16	500 dpi	Hardcopy/ Softcopy	
5	Field data	200 GPS Points		

Field data

Fieldwork was performed to collect the GPS point and to observe the characteristics of land use land cover at Dehradun and its surroundings. Using GPS instrument, we observe land use land cover classes like *dense urban, Mixed urban, Close forest, Open forest, Scrub, Crop land (after harvesting), Cropland (before harvesting), Grassland,* and *wasteland (Dry river), their characteristics and positions* was done and field photographs were taken for interpretation as of polarimetric parameters, for their as training samples for characterization and classification.

Target decomposition and characterisation

Freeman decomposition

Freeman proposed a three-component scattering model in which covariance matrix [C] of polarimetric SAR data is decomposed for information extraction [9]. Freeman decomposition describes scattering mechanisms as due to three physical mechanisms, namely surface scattering, double-bounce scattering and volume scattering:

$$[C] = f_S[C_{surface}] + f_D[C_{double}] + f_V[C_{volume}] \quad (3.1)$$

According to this model, the measured power P may be decomposed into three quantities:

$$P_S = f_S(1+|\beta|^2); P_D = f_D(1+|\alpha|^2); P_V = \frac{8}{3} f_V$$
$$SPAN = P = P_S + P_D + P_V = (|S_{HH}|^2 + 2|S_{HV}|^2 + |S_{VV}|^2) \quad (3.2)$$

The three-component scattering model based on covariance matrix has been successfully applied to decompose PolSAR image under the reflection symmetry condition $\langle S_{HH} S_{HV}^{*} \rangle \approx \langle S_{VV} S_{HV}^{*} \rangle \approx 0$. This method is based on simple physical scattering mechanisms (surface scattering, double-bounce scattering, and volume scattering), just as shown in Fig. 3.1a, the contributions of each of the three scattering mechanisms to the total power are shown for each pixel, with surface scattering colored blue, volume scattering green, and double-bounce scattering red. Result in Fig. 5 shows that volume scattering meets the observation for forest very well. Farmland has surface scattering and double-bounce scattering dominant. This can be interpreted as indication that the longer wavelengths can penetrate the relatively short vegetation in farmland area and the backscatter is mostly from the underlying ground. Therefore, Freeman decomposition can describe different natural targets very good and is powerful for PolSAR image decomposition for natural distributed target areas. However, man-made buildings are also present the volume scattering, thus this model cannot distinguish forest and man-made buildings.

Freeman decompostion ***Krogager decomposition*** ***H/A/α decompostion***

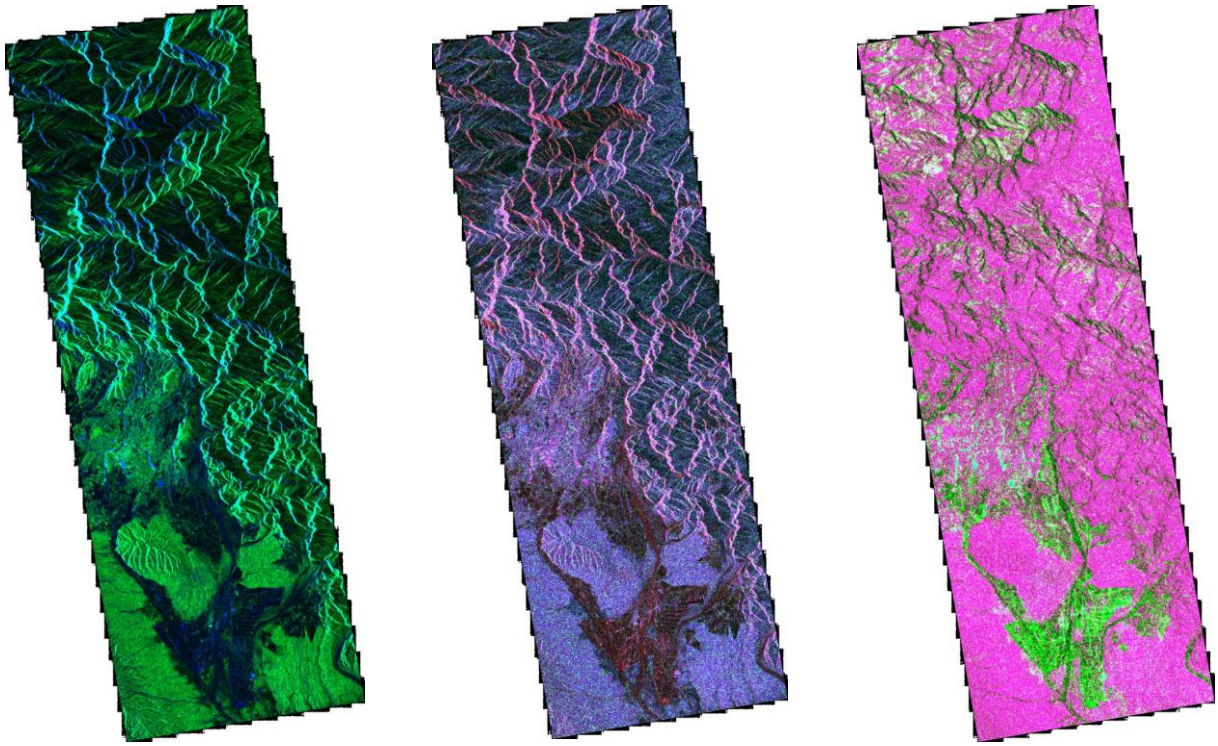

a) ***b)*** ***c)***

Figure 3.1: Image decomposition

Krogager decomposition

According to Krogager, the complex symmetric scattering matrix can be decomposed into three components on the circular basis, which corresponding to a sphere, a diplane and a right- or left-
wound helix, respectively [12]:

$$\begin{aligned}\left[S_{(h,v)}\right] &= e^{j\varphi}\{e^{j\varphi_s}k_s\left[S\right]_s + k_d\left[S\right]_d + k_h\left[S\right]_h\} \\ &= e^{j\varphi}\left\{e^{j\varphi_s}k_s\begin{bmatrix}1 & 0\\ 0 & 1\end{bmatrix} + k_d\begin{bmatrix}\cos 2\theta & \sin 2\theta\\ \sin 2\theta & -\cos 2\theta\end{bmatrix}_d + k_h e^{\mp j2\theta}\begin{bmatrix}1 & \pm j\\ \pm j & 1\end{bmatrix}_h\right\}\end{aligned} \quad (3.3)$$

The phase φ is referred as the absolute phase, whose value depends on the distance between the radar and the target under study. Due to the arbitrary value that this phase can present, it is often considered that the Krogager decomposition presents 5 independent parameters given by $\{\varphi_s, \theta, k_s, k_d, k_h\}$ plus the absolute phase given by φ.
In order to calculate the value of the parameters $\{\varphi_s, \theta, k_s, k_d, k_h\}$ plus the absolute phase φ, a reformulation of (3.3) with the objective to simplify the process is next presented. Now, if we consider the measured scattering matrix expressed in the circular polarization basis (r, l), the Krogager decomposition is then

$$\begin{aligned}\left[S_{(r,l)}\right] &= \begin{bmatrix}S_{rr} & S_{rl}\\ S_{rl} & S_{ll}\end{bmatrix} = \begin{bmatrix}|S_{rr}|e^{j\varphi_{rr}} & |S_{rl}|e^{j\varphi_{rl}}\\ |S_{rl}|e^{j\varphi_{rl}} & |S_{ll}|e^{j\varphi_{ll}}\end{bmatrix} \\ &= e^{j\varphi}\left\{e^{j\varphi_s}k_s\begin{bmatrix}1 & 0\\ 0 & 1\end{bmatrix} + k_d\begin{bmatrix}e^{j2\theta} & 0\\ 0 & -e^{-j2\theta}\end{bmatrix} + k_h e^{\mp j2\theta}\begin{bmatrix}e^{j2\theta} & 0\\ 0 & 0\end{bmatrix}\right\}\end{aligned} \quad (3.4)$$

From (2.4), it can be easily observed that the response of the sphere can be obtained from $|S_{rl}|$

$k_s = |S_{rl}|$ (3.5)

the terms S_{rr} and S_{ll} represent, directly, the diplane component of the decomposition (3.4), but two cases of analysis must be considered according to the difference in absolute value of S_{rr} and S_{ll}. This is necessary in order to accommodate the difference in the scattered power in the right and left circular polarizations. When S_{ll} reprsents the diplane component, it occurs that $|S_{rr}| > |S_{ll}|$. Hence

$$k_d^+ = |S_{ll}| \quad (3.6)$$

$$k_h^+ = |S_{rr}| - |S_{ll}| \quad (3.7)$$

And the helix component presents a left sense. On the contrary, when it is S_{rr} the term which represents the diplane component, it occurs that $|S_{ll}| > |S_{rr}|$.

$$k_d^- = |S_{rr}| \quad (3.8)$$

$$k_h^- = |S_{ll}| - |S_{rr}| \quad (3.9)$$

And the helix has a right sense. Finally, from (3.5), the phase components are

$$\varphi = \frac{1}{2}(\varphi_{rr} + \varphi_{ll} + \pi) \quad (3.10)$$

$$\theta = \frac{1}{2}(\varphi_{rr} - \varphi_{ll} - \pi) \quad (3.11)$$

$$\varphi = \varphi_{rl} - \frac{1}{2}(\varphi_{rr} + \varphi_{ll} + \pi) \quad (3.12)$$

In order to relate the formulations of the Krogager decomposition presented in (3.3) and (3.4), the following relations are useful

$$S_{rr} = jS_{hv} + \frac{1}{2}(S_{hh} - S_{hv}) \quad (3.13)$$

$$S_{ll} = jS_{hv} - \frac{1}{2}(S_{hh} - S_{hv}) \quad (3.14)$$

$$S_{rl} = \frac{j}{2}(S_{hh} + S_{vv}) \quad (3.15)$$

H/A/α decomposition

The eigenvector – eigenvalue based decomposition is based on the eigen decomposition of the coherency matrix $\langle[T_3]\rangle$ [4], [5]. According to the eigen decomposition theorem, the 3x3 Hermitian matrix $\langle[T_3]\rangle$ can be decomposed as follows

$$\langle[T_3]\rangle = [U_3][\sum{}_3][U_3]^{-1} \quad (3.16)$$

The 3x3 real, diagonal matrix $[\Sigma_3]$ contains the eigenvalues $\langle[T_3]\rangle$

$$\langle[\sum\nolimits_3]\rangle = \begin{bmatrix} \lambda_1 & 0 & 0 \\ 0 & \lambda_2 & 0 \\ 0 & 0 & \lambda_3 \end{bmatrix} \qquad (3.17)$$

Where $\infty > \lambda_1 > \lambda_2 > \lambda_3 > 0$

The 3x3 unitary matrix $[U_3]$ contains the eigenvector $\underline{u}_i$ for i = 1, 2, 3 of $\langle[T_3]\rangle$

$$[U]=[\underline{u}_1, \underline{u}_2, \underline{u}_3] \qquad (3.18)$$

The eigenvectors $\underline{u}_i$ for i = 1, 2, 3 of $[T_3]$ can be formulated as follows

$$u_i = \left[\cos\alpha_i \quad \sin\alpha_i \cos\beta_i e^{j\delta_i} \quad \sin\alpha_i \cos\beta_i e^{j\gamma_i}\right]^T \qquad (3.19)$$

Considering the expressions (3.17) and (3.18), the Eigen decomposition of $\langle[T_3]\rangle$, i.e., (3.16), can be written as follows

$$\langle[T_3]\rangle = \sum_{j=1}^{3} \lambda_i u_i u_i^{*T} \qquad (3.20)$$

Where sumbol $*^T$ stands for complex conjugate. As (3.20) shows, the rank 3 matrix $\langle[T_3]\rangle$ can be decomposed as the combination of three rank 1 coherency matrices formed as

$$\langle[T_3]\rangle = u_i u_i^{*T} \qquad (3.21)$$

This can be related to the pure scattering mechanisms given at (3.19).

The eigenvalues (3.17) and the eigenvectors (3.18) are considered as the primary parameters of the eigen decomposition of $\langle[T_3]\rangle$. In order to simplify the analysis of the physical information provided by this eigen decomposition, three secondary parameters are defined as a function of the eigenvalues and the eigenvector of $\langle[T_3]\rangle$:

* Entropy

$$H = -\sum_{j=1}^{3} p_i \log_3(p_i); \; p_i = \frac{\lambda_i}{\sum_{k=1}^{3} \lambda_k} \qquad (3.22)$$

Where p_i, also called the probility of the eigenvalue λ_i, represent the relative importance of this eigenvalue respect to the total scattered power, since

$$\text{SPAN} = |S_{hh}|^2 + |S_{vv}|^2 + 2|S_{hv}|^2 = \sum_{k=1}^{3} \lambda_k \qquad (3.23)$$

* Anisotropy

$$A = \frac{\lambda_2 - \lambda_3}{\lambda_2 + \lambda_3} \qquad (3.24)$$

* Mean alpha angle

$$\underline{\alpha} = \sum_{i=1}^{3} p_i \alpha_i \qquad (3.25)$$

The Eigen decomposition of the coherency matrix is also referred as the H/A/$\underline{\alpha}$ decomposition.

Characterisation and analysis

Mean and standard deviation values were calculated from each training samples of all decompositions. Values were tabulated and graphs for those values were plotted. Using those graph patterns, we identified which parameter plays key roll in classification of Land Use Land Cover classes.

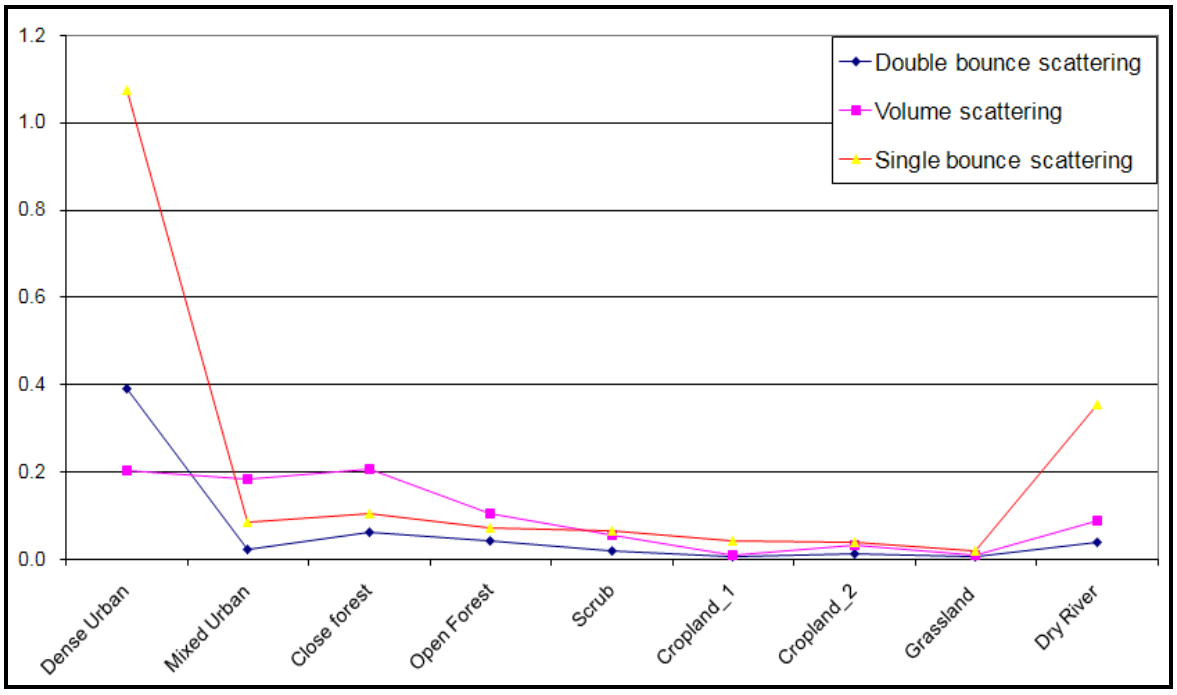

Figure 3.1: Freeman decomposition characterization

It is clear from above trends that volume and single bounce scattering can be used for classification of LULC. Double bounce scattering was not much dominant over different regions so it was not used for identification of different classes.

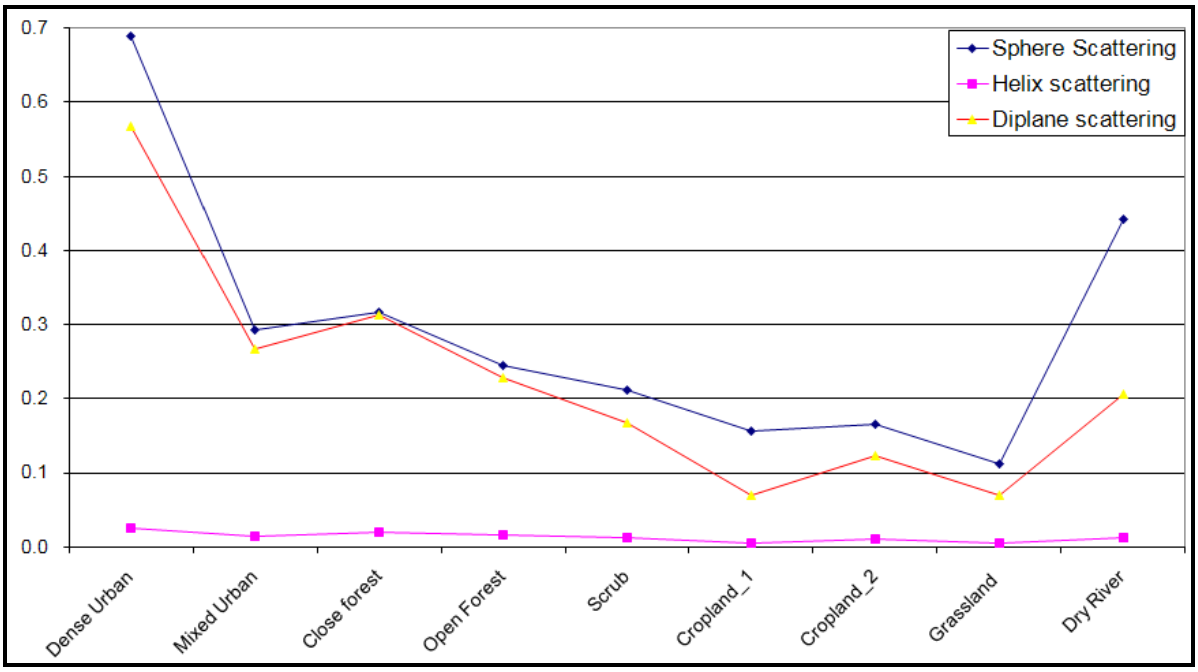

Figure 3.2: Krogager decomposition characterization (25/05/2010)

Helix scattering was observed going flat over all classes so it was neglected for further classification. Sphere scattering and Diplane scattering were showed remarkable difference then Helix over different features so chosen for classification.

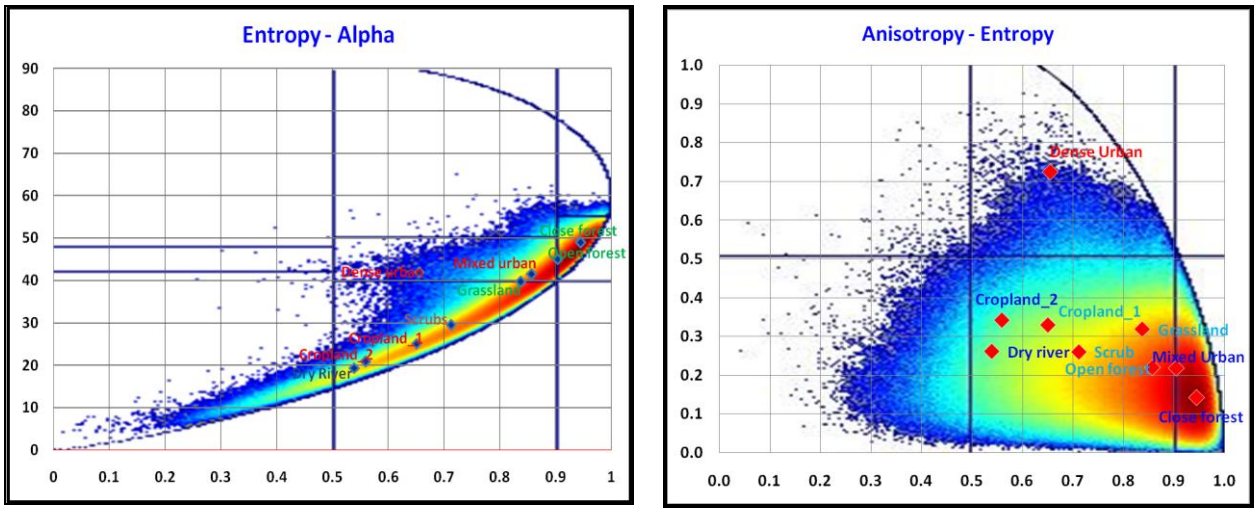

Figure3.3: H/A/α decomposition

Scatter diagram was made by considering Entropy, Alpha and Anisotropy values of different classes. Different zones located from this scatter diagram. It is clear from above the diagram (Entropy-Alpha) that closes forest and open forest falls in single zone. Dense urban and mixed urban belongs to same zone. Remaining all classes was in one zone. Otherwise, the diagram Anisotropy-Entropy shows that dense urban falls in single zone. Mixed urban and close forest belongs to same zone.

Land use Land cover classification using Support vector machine algorithm

Support vector machine algorithm

The SVM is designed for binary-classification problems, assuming the data are linearly separable. Given the training data (x_i , y_i), i = 1, 2, …,l, $x_i \in R^n$, $y_i \in \{+1, -1\}$, where R^n is the input space, x_i is the sample vector and y_i is the class label of x_i, the separating hyperplane (ϖ, b) is a linear discriminating function that solves the optimization problem:

$$\min_{(\varpi,b)} \langle \omega, \varpi \rangle$$

Subject to $y_i(<\varpi,x_i> + b) \geq 1$, i =1, …,l,

Where <.,.> indicates the inner product operation. The minimal distance between the samples and the separating hyperplane, i.e, the margin, is $1/\|\varpi\|$.
In order to relax the margin constraints for the non-linearly separable data, the slack variables are introduced into the optimization problem:

$$\min_{(\xi,\varpi,b)} \langle \omega, \varpi \rangle + C\sum_{i=1}^{l} \xi_i$$

Subject to $y_i(<\varpi,x_i> + b) \geq 1- \xi_i$, i = 1, 2, …,l, $\xi_i \geq 0$.
This leads to a soft margin SVM that is generally discussed and applied. The resulted classifier is called the 1-norm soft margin SVM, and C is the penatly parameter of error. The decision function of the classifier is

$$sign(\sum_{x_i:SV} y_i \alpha_i \langle x_i, x \rangle + b)$$

In practice, since the real data are often not linearly separable in the input space, the data can be mapped into a high dimensional feature space, in which the data are sparse and possibly more separable. The mapping is often not explicitly given. Instead, a kernel function is incorporated to simply the computation of the inner product value of the transformed data in the feature space.
When using a function $\phi : X \rightarrow F$ to map the data in to a high dimensional featurespace, the decision function of the classifier becomes

$$sign(\sum_{x_i:SV} y_i \alpha_i \langle \phi(x_i), \phi(x) \rangle + b)$$

The mapping ϕ is not given explicitly in most cases. Instead, a kernel function $K(x, x') = \langle \phi(x), \phi(x') \rangle$ gives the inner product value of x and x' in the feature space. Choosing a kernel function is therefore choosing a feature space and the decision function becomes

$$sign(\sum_{x_i:SV} y_i \alpha_i K(x_i, x) + b)$$

The generally used kernel functions are

- linear: $K(x, x') = \langle x, x' \rangle$;
- polynomial: $K(x, x') = (\gamma \langle x, x' \rangle + r)^d, \gamma > 0$;
- radial basis function (RBF): $K(x, x') = e^{-\gamma \|x - x'\|^d}, \gamma > 0$;
- sigmoid: $K(x, x') = \tan k(\gamma \langle x, x' \rangle + r)$

For certain parameters, the linear kernel is a special case of RBF kernels [17]. Also, the sigmoid kernel behaves like the RBF kernel [11]. When the data are linearly inseparable, a non-linear kernel that maps the data into the fearture space non-linearly can handle the data better than linear kernels. As the polynomial kernel requires more parameters to be chosen, the RBF kernel is a reasonable first choice of kernel function [8]. When using the RBF kernel, the parameters (d,γ) should be set properly. Generally d is set to be 2. Thus the kernel value is related to the Euclidean distance between the two samples, γ is related to the kernel width.

To apply SVM on multi-class classification problems, the problem can be divided into sub-problems which are binary-classification problems. The often suggested implementations for SVM multi-class classification are the one-against-rest method [13] and the one-against-one method [18]. For an n-class classification problem, the one-against-rest method constructs n SVM models with each one separating a single class with all the other classes, while the one-against-one method constructs n (n-1) classifiers where each one classifies two classes only. Lin et al. [7] showed that the one-against-rest performs best and can be trained faster than the one-against-rest method.

Land use land cover classification and accuracy assessment

Support vector machine algorithm was used for identifying different classes. This algorithm used for all decompositions individually and parameters chosen carefully. Combined parameters also used as input for algorithm for obtaining better and accurate results.

Accuracy assessment should be an important part of any classification. The reason for this is that it usually involves a lot of work in the field, which can be very expensive and time consuming. However, without any accuracy assessment we do not know how accurate our classification is.

The accuracy of a classification is usually assessed by comparing the classification with some reference data that is believed to accurately reflect the true land cover. Sources of reference data include among other things ground truth, higher resolution satellite images, and maps derived from aerial photo interpretation.

The accuracy assessment reflects really the difference between our classification and the reference data.

The results of an accuracy assessment are usually summarized in a confusion matrix.

Freeman decomposition classification

Class	Dense Urban	Mixed Urban	Close forest	Open forest	Scrub	Cropland 1	Cropland 2	Grassland	Dry river	Total	User Acc (%)
Dense Urban	45	1	0	0	0	0	0	0	0	**46**	**97.83**
Mixed Urban	0	**0**	0	0	0	0	0	0	0	**0**	**0**
Close Forest	8	84	216	0	0	0	1	0	0	**309**	**69.9**
Open Forest	1	30	3	132	44	5	66	3	46	**330**	**40**
Scrub	0	0	0	0	**0**	0	0	0	0	**0**	**0**
Crop land_1	0	0	0	0	10	156	91	48	88	**393**	**39.69**
Cropland_2	0	0	0	0	0	0	**0**	0	0	**0**	**0**
Grassland	0	0	0	0	0	0	0	**0**	0	**0**	**0**
Dry river	0	0	0	0	0	0	0	0	**0**	**0**	**0**
Total	**54**	**115**	**219**	**132**	**54**	**161**	**158**	**51**	**134**	**1078**	
Pro Acc (%)	**83.33**	**0**	**98.63**	**100**	**0**	**96.89**	**0**	**0**	**0**		
Overall Accuracy = 50.928%											
Kappa Coefficient = 0.421											

Krogager decomposition classification

Class	Dense Urban	Mixed Urban	Close forest	Open forest	Scrub	Cropland 1	Cropland 2	Grassland	Dry river	Total	User Acc (%)
Dense Urban	50	0	0	0	0	0	0	0	0	**50**	**100**
Mixed Urban	1	76	34	0	0	0	1	0	0	**112**	**67.86**
Close Forest	3	39	185	0	0	0	0	0	0	**227**	**81.5**
Open Forest	0	0	0	128	22	0	33	2	0	**185**	**69.19**
Scrub	0	0	0	4	21	10	36	1	25	**97**	**21.65**
Crop land_1	0	0	0	0	1	135	14	5	20	**175**	**77.14**
Cropland_2	0	0	0	0	0	9	8	0	2	**19**	**42.11**
Grassland	0	0	0	0	0	0	0	43	0	**43**	**100**
Dry river	0	0	0	0	10	7	66	0	87	**170**	**51.18**
Total	**54**	**115**	**219**	**132**	**54**	**161**	**158**	**51**	**134**	**1078**	
Pro Acc (%)	**92.59**	**66.09**	**84.47**	**96.97**	**38.89**	**83.85**	**5.06**	**84.31**	**64.93**		
Overall Accuracy = 67.996%											
Kappa Coefficient = 0.632											

H/A/α decomposition classification

Class	Dense Urban	Mixed Urban	Close forest	Open forest	Scrub	Cropland 1	Cropland 2	Grassland	Dry river	Total	User Acc (%)
Dense Urban	43	7	0	0	0	0	0	0	0	**50**	**86**
Mixed Urban	5	35	0	13	10	0	12	1	1	**77**	**45.45**
Close Forest	0	6	169	16	0	0	5	5	0	**201**	**84.08**
Open Forest	2	52	50	100	10	0	11	18	0	**243**	**41.15**
Scrub	1	0	0	0	4	8	15	1	9	**38**	**10.53**
Crop land_1	0	0	0	0	23	124	58	9	42	**256**	**48.44**
Cropland_2	0	0	0	0	0	6	19	0	10	**35**	**54.29**
Grassland	3	15	0	3	6	1	8	17	0	**53**	**32.08**
Dry river	0	0	0	0	1	22	30	0	72	**125**	**57.6**
Total	**54**	**115**	**219**	**132**	**54**	**161**	**158**	**51**	**134**	**1078**	
Pro Acc (%)	**79.63**	**30.43**	**77.17**	**75.76**	**7.41**	**77.02**	**12.03**	**33.33**	**53.73**		
Overall Accuracy = 54.082%											
Kappa Coefficient = 0.470											

Decomposition parameters selection classification

Class	Dense Urban	Mixed Urban	Close forest	Open forest	Scrub	Cropland 1	Cropland 2	Grassland	Dry river	Total	User Acc (%)
Dense Urban	44	6	0	0	0	0	0	0	0	**50**	**88**
Mixed Urban	8	92	18	0	0	0	1	0	0	**119**	**77.31**
Close Forest	2	17	201	0	0	0	0	0	0	**220**	**91.36**
Open Forest	0	0	0	130	19	0	22	14	1	**186**	**69.89**
Scrub	0	0	0	0	18	17	43	0	22	**100**	**18**
Crop land_1	0	0	0	0	3	126	27	9	13	**178**	**70.79**
Cropland_2	0	0	0	0	5	4	29	0	15	**53**	**54.72**
Grassland	0	0	0	2	3	0	3	28	0	**36**	**77.78**
Dry river	0	0	0	0	6	14	33	0	83	**136**	**61.03**
Total	**54**	**115**	**219**	**132**	**54**	**161**	**158**	**51**	**134**	**1078**	
Pro Acc (%)	**81.48**	**80**	**91.78**	**98.48**	**33.33**	**78.26**	**18.35**	**54.9**	**61.94**		
Overall Accuracy = 69.666%											
Kappa Coefficient = 0.651											

RESULTS

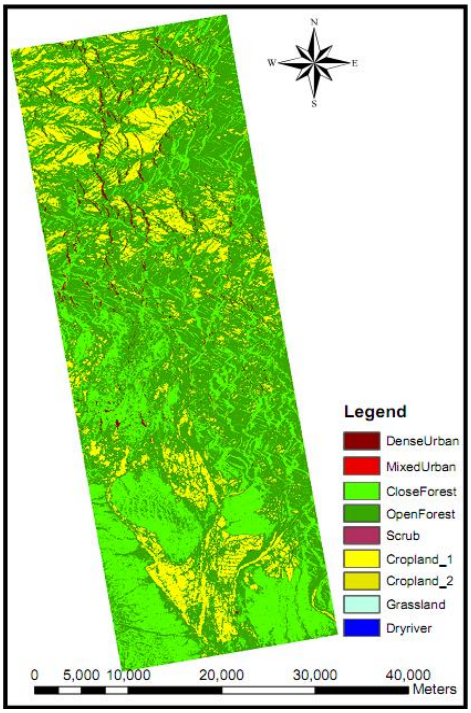

a

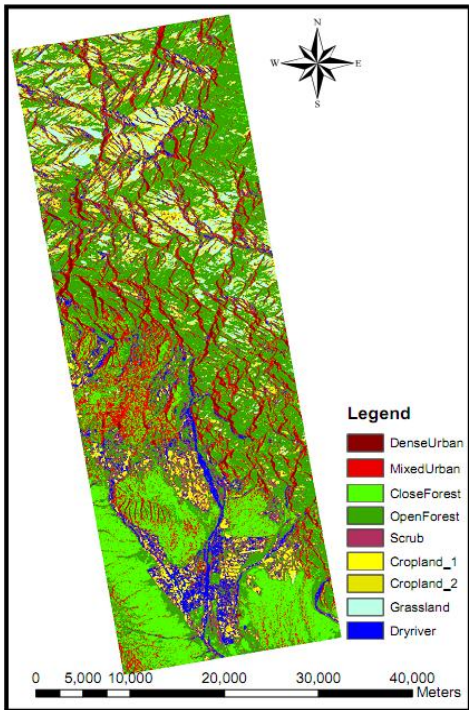

b

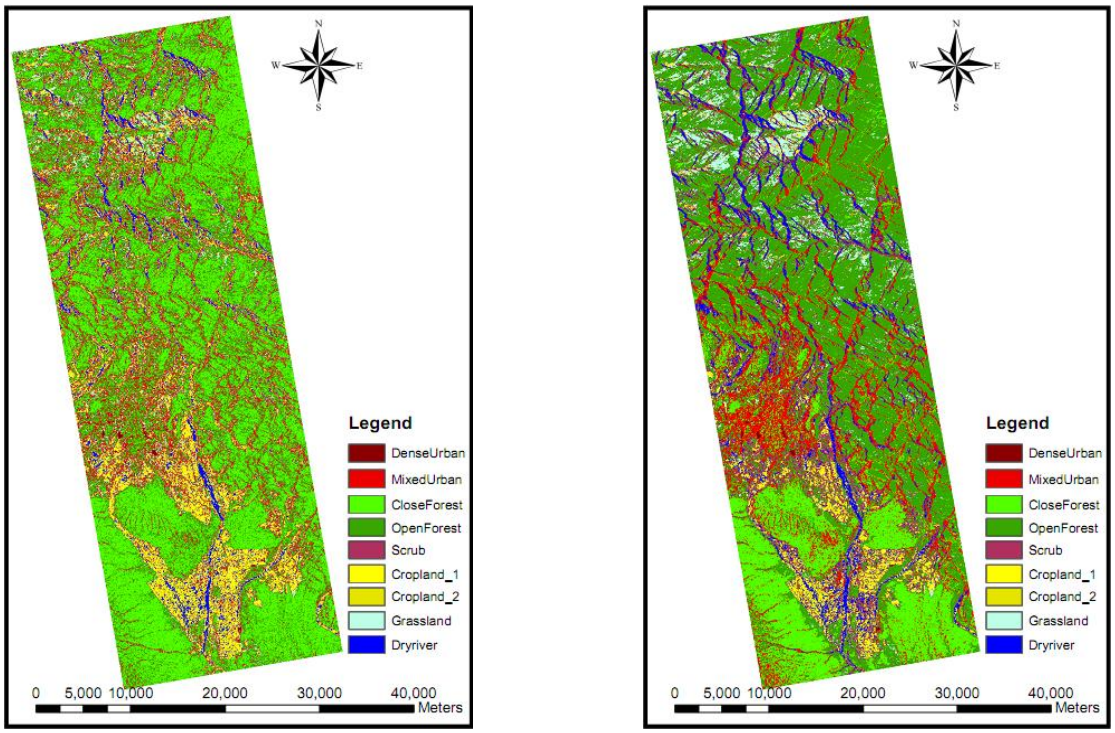

c d

Figure 4.1: Classification images

a) Freeman decomposition; b) Krogager decomposition

c) H/A/α decomposition; d) Decomposition parameters selection

CONCLUSION

In Freeman decomposition, single bounce, double bounce and volume scattering of the targets are separated: Dense urban, close forest, and crop land (before cut) show distinct scattering properties and can be separated well. But, other LU-LC classes could not be separated.

In Krogager (SDH) decomposition, simple (sphere), double bounce (diplane), and multiple (helix) scattering of the targets may be separated. Although, helix scattering is insignificant, well-pronounced simple and double scattering are able to separate majority of the LU-LC classes except scrubs and crop land (after cut).

In Cloude-Pottier H/A/α decomposition, the nature of the scatterers are highlighted in addition to the scattering processes, namely, randomness of scattering and secondary scattering from the target:

- *Most of the classes represent predominant surface scattering except close forest, open forest and mixed urban (grass land – marginal case) with volume scattering.*
- *Mixed urban, close forest, open forest and grass land with high entropy represent distributed target;*
- *Dense urban having low entropy but high anisotropy is more close to pure target with equally important single bounce and double bounce scattering.*

InSAR coherence parameter was not found very useful for separating the LU-LC classes due to longer wavelength of L-band PALSAR data.

Based on the characterization of decomposed parameters, a set of parameters highlighting the scattering properties of the LU-LC classes were selected for classification.

Field samples were collected for each of the LU-LC classes and signatures were generated for classification by Support Vector Machine Algorithm.

Some of the individual LU-LC classes can be well classified using the parameters from individual polarimetric decomposition. However, all the LU-LC classes in totality can be separated well using selected decomposition parameters (odd bounce and volume scattering from Freeman decomposition, sphere and diplane from Krogager decomposition, and entropy, alpha and anisotropy from Cloude-Pottier decomposition) in combination with a classification accuracy of ~70% with a kappa coefficient 0.65.

PolSAR decomposition parameter in combination enables to address Level-2 LU-LC Classification by SVM Algorithm which is otherwise difficult.

Acknowledgement

I am very grateful to Dr R.S Chatterjee, *Geoscience Division, Indian Institute of Remote Sensing, Dehradun, India* (IIRS), Dr P.S Roy, Dean of IIRS and Director of CSSTEAP, Dr S.K Saha Course Director of CSSTEAP, Ms Tran Thi Huong Giang, Hanoi university of Mining and Geology for their cooperation during the project work. Especially, many thanks to the **NAFOSTED (National Foundation for Science and Technology Development** http://www.nafosted.gov.vn/**)** supplied financial for me to attend this conference.

Reference

[1] Alberga, V., 2007. A study of land cover classification using polarimetric SAR parameters. International Journal of Remote Sensing, 28(17), pp. 3851-3870.

[2] Barnes, C. F. and Burki, J., 2006. Late-season rural land-cover estimation with polarimetric-SAR intensity pixel blocks and sigma-tree-structured near-neighbor classifiers. IEEE Transactions on Geoscience and Remote Sensing, 44(9), pp. 2384-2392.

[3] Borghys, D., Y. Yvinec, C. Perneela, A. Pizurica and W. Philips, 2006. Supervised feature-based classification of multi-channel SAR images, Pattern Recognition Letters, 27(4): pp: 252-258.

[4] Cloude, S. R. and Pottier, E., 1996. A review of target decomposition theorems in radar polarimetry. IEEE Transactions on Geoscience and Remote Sensing, 34(2), pp. 498-518.

[5] Cloude, S. R. and Pottier, E., 1997. An entropy based classification scheme for land applications of polarimetric SAR. IEEE Transactions on Geoscience and Remote Sensing, 35(1), pp. 68-78.

[6] Crawford, M.M., S. Kumar, M.R. Ricard, J.C. Gibeaut and A. Neuenschwander, 1999. Fusion of airborne polarimetric and interferometric SAR for classification of coastal environments, IEEE Transactions on Geoscience and Remote Sensing, 37(3): pp. 1306-1315.

[7] C.-W.Hsu, C.-J.Lin, A comparison of methods formulti-class support vector machines, IEEETrans. NeuralNetworks 13(2) (2002) 415-425.

[8]C.-W.Hsu, C.-C.Chang, C.-J.Lin, A practical guide to support vector classification.[Online] Available from World Wide Web: http://www.csie.ntu.edu.tw/cjlin/libsvm.

[9] Freeman, A. and Durden, S. L., 1998. A three-component scattering model for polarimetric SAR data. IEEE Transactions on Geoscience and Remote Sensing, 36(3), pp. 963-973.

[10] Hong, S., Moon, W. M., Paik, H. Y., Choi, G. H., 2002. Data fusion of multiple polarimetricSAR images using discrete wavelet transform (DWT), in Proceedings of IGARSS'02, Toronto, Canada, pp. 3323-3325.

[11]H.-T.Lin, C.-J.Lin, A study on sigmoid kernels for SVM and the training of non- PSD kernels by SMO-type methods, Technical Report,Department of Computer Science and Information Engineering, National Taiwan University.

[12] Krogager, E., 1990. New Decomposition of the Radar Target Scattering Matrix, Electronics Letters, 26(18): pp. 1525-1527.

[13] L.Bottou, C.Cortes, J.Denker, H.Drucker, I.Guyon, L.Jackel, Y.LeCun, U.Muller, E.Sackinger, P.Simard, V.Vapnik, Comparison of classifier methods: A case study in handwritten digit recognition, in: Proceedings of International Conferenceon Pattern Recognition, 1994, pp.77-87.

[14] Lee, J. S. and Pottier, E., 2009. Polarimetric Radar Imaging from Basics to Applications. (p. 180). CRC Press, New York.

[15] Pottier, E. and Lee, J. S., 2000. Application of the "H/A/Alpha" polarimetric decomposition theorem for unsupervised classification of fully polarimetric SAR data based on the Wishart distribution. CEOS SAR Workshop, Toulouse, France, 450, pp. 335-340.

[16] Shimoni, M., D. Borghys, R. Heremans, C. Perneel and M. Acheroy, 2009. Fusion of PolSAR and PolInSAR data for land cover classification, International Journal of Applied Earth Observation and Geoinformation, 11(3): pp. 169-180.

[17] S.S.Keerthi, C.-J.Lin, A symptotic behaviors of support vector machines with Gaussian kernel, Neural Comput. 15(7) (2003)1667-1689.

[18] U.Kreolkopf, C.J.C.Burges, A.J.Smola (Eds.), Advances in Kernel Methods Support Vector Learning, MITPress, Cambridge, MA, 1999.